Available online at www.sciencedirect.com
ScienceDirect
Journal of Computational Physics 223 (2007) 235–249
JOURNAL OF COMPUTATIONAL PHYSICS
www.elsevier.com/locate/jcp

Geometric curve flows on parametric manifolds

Alon Spira *, Ron Kimmel

Department of Computer Science, Technion—Israel Institute of Technology, Technion City, Haifa 32000, Israel

Received 5 September 2005; received in revised form 7 September 2006; accepted 12 September 2006
Available online 27 October 2006

Abstract

Planar geometric curve evolution equations are the basis for many image processing and computer vision algorithms. In order to extend the use of these algorithms to images painted on manifolds it is necessary to devise numerical schemes for the implementation of the geodesic generalizations of these equations.

We present efficient numerical schemes for the implementation of the classical geodesic curve evolution equations on parametric manifolds. The efficiency of the schemes is due to their implementation on the parameterization plane rather than on the manifold itself. We demonstrate these flows on various manifolds and use them to implement two applications: scale space of images painted on manifolds and segmentation by an active contour model.

Keywords: Curve; Flow; Manifold; Parametric

1. Introduction

The motion of curves and images in $\mathbb{R}^2$ has been researched extensively. There are many applications in image processing and computer vision, such as scale space by linear and nonlinear diffusions [1–4], image enhancement through anisotropic diffusions [3,5–8] and image segmentation by active contours [9–12]. The level set formulation [13] has provided good means to implement these flows. Extending these motions to manifolds embedded in spaces of higher dimensions can be beneficial for many applications.

Some of the previous work dealt with specific flows. Geodesic curvature flow on manifolds constructed from patches homeomorphic to $\mathbb{R}^2$ was implemented by [14]. A similar flow was used on manifolds that are graphs of functions ($\{x, y, z(x, y)\}$) to find shortest paths [15,16] and to construct an intrinsic scale space for images on surfaces [17]. The same flow was implemented also on triangulated manifolds [18]. All the above, except for the last, were implemented by projecting the PDEs to $\mathbb{R}^2$, performing the numerical calculations there and then mapping back the solutions to the manifold.

A more general approach for the motion of curves on manifolds was developed by Cheng et al. [19] and Bertalmio et al. [20]. In [19] many geometric flows are implemented and in [20] various PDEs and variational

* Corresponding author.
E-mail addresses: salon@cs.technion.ac.il (A. Spira), ron@cs.technion.ac.il (R. Kimmel).

0021-9991/$ - see front matter
doi:10.1016/j.jcp.2006.09.008

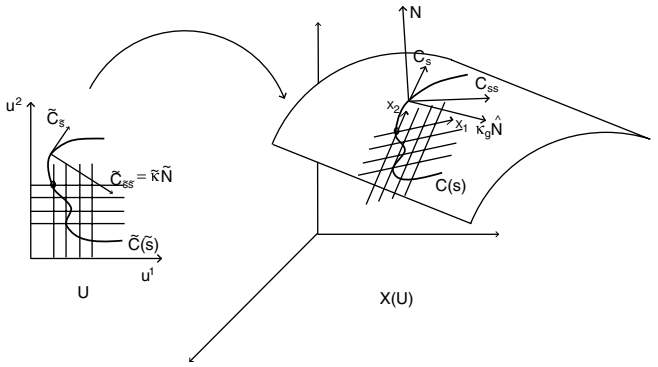

Fig. 1. The curve $C(s)$ on the manifold $X(U)$ and its origin $\widetilde{C}(\tilde{s})$ on the parameterization plane U.

problems are solved, both for general manifolds. Their approach is to implicitly represent both the manifold and the curve or data on it as level sets of functions in $\mathbb{R}^N$. The level set representing the manifold is static and the level set representing the curve or the data is moving according to the PDE. This approach has several drawbacks. It necessitates the extension of the manifold and the curve or data on it to functions in $\mathbb{R}^N$. The calculations are done in $\mathbb{R}^N$ and might be computationally prohibitive for $N > 3$. Finally, the method is restricted to manifolds that can be represented by a level set function, excluding more general manifolds, such as self-intersecting ones.

We present efficient numerical schemes for the implementation of various flows on parametric manifolds.[1] We solve the problems arising from the implicit representation approach described in the previous paragraph by following in the footsteps of the first approach of working on the parameterization plane. Namely, we back project the flow from the manifold to the parameterization plane, solve it on this plane and then map the result back to the manifold. The complexity of the calculations is not affected by the dimension of the space in which the manifold is embedded and the approach is suited for all manifolds, including self-intersecting ones.

We consider a parameterization plane $U = \{u^1, u^2\} \in \mathbb{R}^2$. This plane is mapped by $X : \mathbb{R}^2 \to \mathbb{R}^N$ to the parametric manifold $X(U) = \{x^1(u^1, u^2), x^2(u^1, u^2), \ldots, x^N(u^1, u^2)\} \in \mathbb{R}^N$. Any curve $C(s) \in X(U)$ has an origin $\widetilde{C}(\tilde{s}) \in U$, i.e. each point $p \in C(s)$ is a mapping of a corresponding point $\tilde{p} \in \widetilde{C}(\tilde{s})$ given by $p = X(\tilde{p})$. s and $\tilde{s}$ are the arc length parameterizations of the curves C and $\widetilde{C}$, respectively. The derivatives of X with respect to u^i are defined as $X_i \triangleq \frac{\partial X}{\partial u^i}$. See Fig. 1.

The distance element on the manifold is

$$ds = \sqrt{g_{ij} du^i du^j}, \tag{1}$$

where we use Einstein's summation convention and the (covariant) metric tensor of the manifold g_{ij} is calculated by

$$(g_{ij}) = \begin{pmatrix} g_{11} & g_{12} \\ g_{21} & g_{22} \end{pmatrix} = \begin{pmatrix} X_1 \cdot X_1 & X_1 \cdot X_2 \\ X_2 \cdot X_1 & X_2 \cdot X_2 \end{pmatrix}. \tag{2}$$

g^{ij} are the components of the contravariant metric tensor (the inverse of the covariant metric tensor) and $g = \det(g_{ij}) = g_{11}g_{22} - g_{12}^2$.

According to the above definitions, the derivative of $C(s)$ with respect to its arc length is C_s, which is the tangent to the curve C. Similarly, we have $\widetilde{C}_{\tilde{s}}$, which is the tangent to $\widetilde{C}(\tilde{s})$. We denote by N the normal to the plane tangent to the manifold $X(U)$ and in the direction of $X_1 \times X_2$. $\widehat{N}$ is the unit vector normal to the curve $C(s)$ lying in that plane. $\widetilde{N}$ represents the normal to $\widetilde{C}_{\tilde{s}}$ in the plane U.

This paper is organized as follows. Section 2 shows how the geodesic flows are projected onto the parameterization plane. The level set representation of the flows on the parameterization plane and the numerical

[1] For completeness sake, we include here results that where first presented in [21,22].

schemes used to implement them are described in Sections 3 and 4, respectively. In Section 5, the flows are demonstrated on various manifolds. Section 6 presents two application for the flows: a geometric scale space for images painted on manifolds and the segmentation of these images by an extension of the geodesic active contour model. Conclusions appear in Section 7.

2. Translating flows on manifolds to flows on the parameterization plane

Any geometric flow of the curve $C(s)$ of the form $C_t = F\widehat{N}$, has a corresponding geometric flow on U of the form $\widetilde{C}_t = \widetilde{F}\widetilde{N}$. If we can find $\widetilde{F}$ as a function of F and the mapping X, we can simplify the calculation of the flow on $X(U)$ by performing the flow on U and then mapping the result onto $X(U)$. To enable this, we represent vectors in the N-dimensional space according to the basis $\{X_1, X_2\}$. The other components of the vectors, which are perpendicular to X_1 and X_2, do not affect the geometric flow of the curve $C(s)$ on the manifold $X(U)$.

2.1. Geodesic curvature flow

We start with the geodesic curvature flow of $C(s)$

$$C_t = \kappa_g \widehat{N} = C_{ss} - \langle C_{ss}, N\rangle N. \tag{3}$$

This is the flow of the curve $C(s)$ according to the component of its curvature, tangent to the surface $X(U)$. Taking only this component of the curvature keeps the curve on the manifold. See Fig. 2.

The representation of C_s according to the basis $\{X_1, X_2, N\}$ is

$$C_s = u_s^i X_i. \tag{4}$$

By differentiating this expression with respect to s we get

$$C_{ss} = u_{ss}^i X_i + u_s^i(\Gamma_{ij}^k X_k + b_{ij}N)u_s^j \tag{5}$$

with Γ_{ij}^k being Christoffel's symbols and b_{ij} the coefficients of the second fundamental form [23]. $\kappa_g\widehat{N}$ is the component of C_{ss} in the plane tangent to $X(U)$, i.e. the covariant derivative of C_s. We get it by discarding the component of C_s in the direction of N

$$\kappa_g \widehat{N} = \frac{\mathrm{D}C_s(s)}{\mathrm{d}s} = u_{ss}^i X_i + \Gamma_{ij}^k X_k u_s^i u_s^j = (u_{ss}^k + \Gamma_{ij}^k u_s^i u_s^j)X_k. \tag{6}$$

If $C(s)$ is a geodesic, then by definition $\frac{\mathrm{D}C_s(s)}{\mathrm{d}s} = 0$, and Eq. (3) becomes $C_t = 0$. This is the stopping point of the geodesic curvature flow.

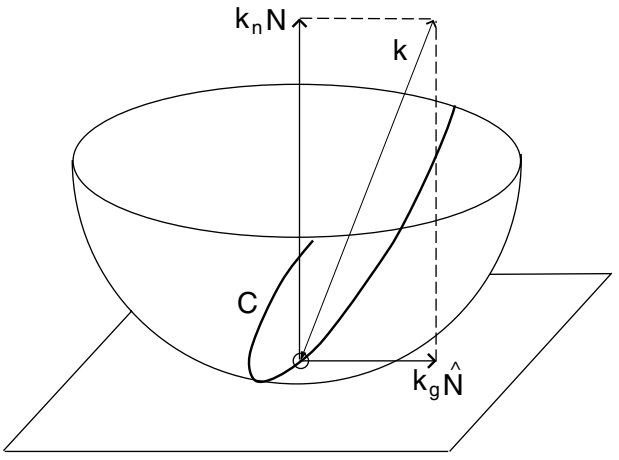

Fig. 2. The curvature has two orthogonal components: the normal curvature and the geodesic curvature.

We use the chain rule to compute C_t

$$C_t = X_k u_t^k. \tag{7}$$

Combining this result with Eqs. (3) and (6) yields

$$u_t^k = u_{ss}^k + \Gamma_{ij}^k u_s^i u_s^j \tag{8}$$

or

$$\widetilde{C}_t = \widetilde{C}_{ss} + \{\Gamma_{ij}^1 u_s^i u_s^j, \Gamma_{ij}^2 u_s^i u_s^j\}. \tag{9}$$

In order to write this equation as a function of $\tilde{s}$ instead of s, we use

$$s = \int |C_{\tilde{s}}| \, \mathrm{d}\tilde{s} \;\Rightarrow\; q \triangleq \frac{\partial \tilde{s}}{\partial s} = |C_{\tilde{s}}|^{-1} = |X_i u_{\tilde{s}}^i|^{-1} = (X_i X_j u_{\tilde{s}}^i u_{\tilde{s}}^j)^{-\frac{1}{2}} = (g_{ij} u_{\tilde{s}}^i u_{\tilde{s}}^j)^{-\frac{1}{2}}, \tag{10}$$

where we replaced $X_i X_j$ in q with g_{ij}, which are the components of the metric tensor. We get

$$u_s^i = \frac{\partial \tilde{s}}{\partial s} u_{\tilde{s}}^i = q u_{\tilde{s}}^i \tag{11}$$

and

$$u_{ss}^i = q_s u_{\tilde{s}}^i + q u_{\tilde{s}\tilde{s}}^i = q_s u_{\tilde{s}}^i + q^2 u_{\tilde{s}\tilde{s}}^i. \tag{12}$$

Using these relations in Eq. (9) yields

$$\widetilde{C}_t = q_s C_{\tilde{s}} + q^2 (C_{\tilde{s}\tilde{s}} + \{\Gamma_{ij}^1 u_{\tilde{s}}^i u_{\tilde{s}}^j, \Gamma_{ij}^2 u_{\tilde{s}}^i u_{\tilde{s}}^j\}), \tag{13}$$

but the geometric flow depends only on the component of $\widetilde{C}_t$ in the direction of $\widetilde{N}$, i.e.

$$\langle \widetilde{C}_t, \widetilde{N} \rangle = q^2 (\tilde{\kappa} + \langle \{\Gamma_{ij}^1 u_{\tilde{s}}^i u_{\tilde{s}}^j, \Gamma_{ij}^2 u_{\tilde{s}}^i u_{\tilde{s}}^j\}, \widetilde{N} \rangle) = \frac{\tilde{\kappa} + \langle \{\Gamma_{ij}^1 u_{\tilde{s}}^i u_{\tilde{s}}^j, \Gamma_{ij}^2 u_{\tilde{s}}^i u_{\tilde{s}}^j\}, \widetilde{N} \rangle}{g_{ij} u_{\tilde{s}}^i u_{\tilde{s}}^j}, \tag{14}$$

where $\tilde{\kappa}$ is the curvature of $\widetilde{C}$.

We can compare this result with the result in [17] by defining $X = \{x, y, z(x, y)\}$. We calculate Γ_{ij}^k in this case by

$$\Gamma_{ij}^k = X_{ij} X^k, \tag{15}$$

where X^k is the contravariant version of the covariant vector X_k, calculated by

$$X^k = g^{kj} X_j. \tag{16}$$

This results in

$$\Gamma_{ij}^k = \frac{z_{ij} z_k}{g}. \tag{17}$$

Inserting this expression for Γ_{ij}^k in Eq. (14) yields

$$\langle \widetilde{C}_t, \widetilde{N} \rangle = \frac{\tilde{\kappa} + \langle \frac{z_{ij}}{g} u_{\tilde{s}}^i u_{\tilde{s}}^j \{z_1, z_2\}, \widetilde{N} \rangle}{g_{ij} u_{\tilde{s}}^i u_{\tilde{s}}^j}, \tag{18}$$

which can be easily shown to be equivalent to the expression in [17].

2.2. Geodesic constant flow

The next flow we deal with is the geodesic constant flow of $C(s)$

$$C_t = F \widehat{N}, \tag{19}$$

where F is the velocity of the curve in the direction normal to the curve and tangent to the manifold $X(U)$.

Because $\widehat{N}$ is tangent to the manifold $X(U)$, it can be represented according to the basis $\{X_1, X_2\}$

$$\widehat{N} = a^i X_i. \tag{20}$$

We need two conditions in order to find the two coefficients a^i. The first condition is that $\widehat{N}$ is perpendicular to C_s, that is

$$\langle C_s, \widehat{N} \rangle = 0. \tag{21}$$

The second condition is that $\widehat{N}$ is a unit vector

$$\langle \widehat{N}, \widehat{N} \rangle = 1. \tag{22}$$

Using the representations of C_s and $\widehat{N}$ according to the basis $\{X_1, X_2\}$ in Eqs. (21) and (22) yields

$$\begin{cases} a^i u_s^j g_{ij} = 0, \\ a^i a^j g_{ij} = 1. \end{cases} \tag{23}$$

Solving these equations and using Eq. (11) yields

$$a^1 = \frac{q}{g^{\frac{1}{2}}}\left(u_s^1 g_{12} + u_s^2 g_{22}\right), \quad a^2 = -\frac{q}{g^{\frac{1}{2}}}\left(u_s^1 g_{11} + u_s^2 g_{12}\right). \tag{24}$$

The resulting equation for the flow is

$$\widetilde{C}_t = \frac{Fq}{g^{\frac{1}{2}}}\{u_s^1 g_{12} + u_s^2 g_{22}, -u_s^1 g_{11} - u_s^2 g_{12}\} \tag{25}$$

and the corresponding geometric normal velocity on U is

$$\langle \widetilde{C}_t, \widetilde{N} \rangle = \frac{Fq}{g^{\frac{1}{2}}}\langle \{u_s^1 g_{12} + u_s^2 g_{22}, -u_s^1 g_{11} - u_s^2 g_{12}\}, \widetilde{N} \rangle. \tag{26}$$

2.3. Geodesic advection

The last flow is the geodesic advection of $C(s)$

$$C_t = V, \tag{27}$$

where V is an external vector field, i.e. V is independent of the curve $C(s)$.

The representation of V according to the basis $\{X_1, X_2\}$ is

$$V = b^i X_i. \tag{28}$$

The scalar products between V and the vectors X_i are

$$v_i \triangleq \langle V, X_i \rangle = b^j g_{ij}. \tag{29}$$

A few manipulations yield

$$b^1 = \frac{v_1 g_{22} - v_2 g_{12}}{g}, \quad b^2 = \frac{v_2 g_{11} - v_1 g_{12}}{g}. \tag{30}$$

The resulting equation for the flow is

$$\widetilde{C}_t = \{v_1 g^{11} + v_2 g^{12}, v_2 g^{22} + v_1 g^{12}\}. \tag{31}$$

This flow is an advection on the parameterization plane.

3. Level set representation of the flows

We next convert the flow equations we got in the previous section into level set equations [13]. This formulation enjoys many numerical advantages.

According to this formulation, the curve evolution equation

$$\langle \widetilde{C}_t, \widetilde{N} \rangle = E \tag{32}$$

is replaced by the level set equation

$$\phi_t = E|\nabla\phi|. \tag{33}$$

3.1. Geodesic curvature flow

For the geodesic curvature flow this means converting Eq. (14) to a level set formulation. We assume that $\widetilde{C}(\tilde{s}) = \{u^1(\tilde{s}), u^2(\tilde{s})\}$ is the zero set of $\phi(u^1, u^2)$ and use the relation

$$\{-u^2_{\tilde{s}}, u^1_{\tilde{s}}\} = \widetilde{N} = \frac{\nabla\phi}{|\nabla\phi|}, \tag{34}$$

to get

$$u^1_{\tilde{s}} = \frac{\phi_2}{(\phi_1^2+\phi_2^2)^{\frac{1}{2}}}, \quad u^2_{\tilde{s}} = \frac{-\phi_1}{(\phi_1^2+\phi_2^2)^{\frac{1}{2}}} \tag{35}$$

and

$$\tilde{\kappa} = \operatorname{div}\left(\frac{\nabla\phi}{|\nabla\phi|}\right) = \frac{\phi_1^2\phi_{22} - 2\phi_1\phi_2\phi_{12} + \phi_2^2\phi_{11}}{(\phi_1^2+\phi_2^2)^{\frac{3}{2}}}. \tag{36}$$

Putting all this together leads to:

$$\begin{aligned}
\phi_t &= \frac{\phi_1^2\phi_{22} - 2\phi_1\phi_2\phi_{12} + \phi_2^2\phi_{11}}{g_{22}\phi_1^2 - 2g_{12}\phi_1\phi_2 + g_{11}\phi_2^2} + \frac{\Gamma^1_{22}\phi_1^3 + (\Gamma^2_{22} - 2\Gamma^1_{12})\phi_1^2\phi_2 + (\Gamma^1_{11} - 2\Gamma^2_{12})\phi_1\phi_2^2 + \Gamma^2_{11}\phi_2^3}{g_{22}\phi_1^2 - 2g_{12}\phi_1\phi_2 + g_{11}\phi_2^2} \\
&= \frac{(-1)^{(i-j)}\phi_i\phi_j\phi_{(3-i)(3-j)}}{gg^{\alpha\beta}\phi_\alpha\phi_\beta} + \frac{(-1)^{(i-j)}\Gamma^k_{ij}\phi_{(3-i)}\phi_{(3-j)}\phi_k}{gg^{\alpha\beta}\phi_\alpha\phi_\beta} \\
&= \frac{(-1)^{(i-j)}\phi_i\phi_j\phi_{(3-i)(3-j)}}{g|\nabla_M\phi|^2} + \frac{(-1)^{(i-j)}\Gamma^k_{ij}\phi_{(3-i)}\phi_{(3-j)}\phi_k}{g|\nabla_M\phi|^2}
\end{aligned} \tag{37}$$

with Christoffel's symbols calculated by derivatives of the first fundamental form

$$\Gamma^k_{ij} = \frac{1}{2}g^{kl}(\partial_i g_{lj} + \partial_j g_{il} - \partial_l g_{ij}). \tag{38}$$

If the manifold is a plane, we expect the geodesic curvature flow to become the curvature flow. In this case, $g_{11} = g_{22} = 1$, $g_{12} = 0$ and $\Gamma^k_{ij} = 0,\ \forall i,j,k$, and we get

$$\phi_t = \frac{\phi_1^2\phi_{22} - 2\phi_1\phi_2\phi_{12} + \phi_2^2\phi_{11}}{\phi_1^2+\phi_2^2}, \tag{39}$$

which is the level set formulation of the curvature flow.

3.2. Geodesic constant flow

The next flow is the geodesic constant flow. First, we use Eq. (34) in Eq. (26) to get

$$\langle \widetilde{C}_t, \widetilde{N} \rangle = \frac{F}{qg^{\frac{1}{2}}} \tag{40}$$

and then convert this flow into a level set representation by using Eqs. (25) and (35) that yield

$$\phi_t = -Fg^{\frac{1}{2}}(g^{ij}\phi_i\phi_j)^{\frac{1}{2}} = -Fg^{\frac{1}{2}}\|\nabla_M\phi\|, \tag{41}$$

with $\nabla_M\phi$ being the gradient of ϕ on the manifold M.

If the manifold is a plane, $g = g^{11} = g^{22} = 1$ and $g^{12} = 0$. Eq. (41) becomes

$$\phi_t = -F(\phi_1^2 + \phi_2^2)^{\frac{1}{2}} = -F\|\nabla\phi\|, \tag{42}$$

which is the level set formulation of the constant flow on a plane.

3.3. Geodesic advection

The level set representation of the planar flow equation

$$\widetilde{C}_t = \widetilde{V} \tag{43}$$

is

$$\phi_t = \langle\widetilde{V}, \nabla\phi\rangle. \tag{44}$$

Therefore, the level set representation of Eq. (31) is

$$\phi_t = (v_1 g^{11} + v_2 g^{12})\phi_1 + (v_2 g^{22} + v_1 g^{12})\phi_2. \tag{45}$$

If the manifold is a plane, $X(U) = \{u^1, u^2, \text{const}\}$ so $X_1 = \{1,0,0\}$ and $X_2 = \{0,1,0\}$. $v_i = V^i$ (the components of V) and Eq. (45) becomes Eq. (27) as expected.

4. Numerical schemes for the level set equations

The implementation of the level set equations on the parameterization plane necessitates appropriate numerical schemes. These schemes are presented in this section.

4.1. Geodesic curvature flow

We start with a numerical scheme for Eq. (37). The first term on the right-hand side of this equation is diffusive and can be implemented with central differences. The second term is a non-convex hyperbolic term and needs a special numerical scheme.

We used a fifth-order weighted essentially non-oscillatory (WENO) scheme with a global Lax–Friedrichs (LF) flux in space [24] and a third-order total variation diminishing Runge–Kutta (TVD-RK) scheme in time [25]. Non-periodic boundary conditions were used.

A re-distancing of the level set function was activated every few iterations, as a regularizing process. The re-distancing was accomplished by the Sussman–Fatemi method [26]. This method uses the equation

$$\phi_t = \text{sign}(\phi_0)(1 - |\nabla\phi|) \tag{46}$$

to transform the level set function ϕ_0 into a distance map. Also this equation is implemented by a fifth-order WENO-LF, third order TVD-RK numerical scheme. The zero set of ϕ_0 is maintained by applying a volume conserving condition of the form

$$\partial_t \int_\Omega H(\phi) = 0 \tag{47}$$

with H the Heaviside function and Ω a fixed domain. The condition is applied by using a gradient projection step.

4.2. Geodesic constant flow

In order to implement Eq. (41) which is the level set formulation of the geodesic constant flow, we propose an extension of the numerical scheme used in [27] for shape from shading

$$|\nabla\phi| \approx [\max^2(D_x^-\phi, -D_x^+\phi, 0) + \max^2(D_y^-\phi, -D_y^+\phi, 0)]^{\frac{1}{2}}. \tag{48}$$

In our case we use

$$\nabla_M\phi| \approx [g^{11}\max^2(D_{u^1}^-\phi, -D_{u^1}^+\phi, 0) + 2g^{12}\,\mathrm{minmod}(D_{u^1}^-\phi, D_{u^1}^+\phi)\,\mathrm{minmod}(D_{u^2}^-\phi, D_{u^2}^+\phi) + g^{22}\max^2(D_{u^2}^-\phi, -D_{u^2}^+\phi, 0)]^{\frac{1}{2}} \tag{49}$$

with $D_{u^i}^-$ the backward difference in the u^i direction, $D_{u^i}^+$ the forward difference in the same direction and

$$\mathrm{minmod}(a,b) = \frac{[\mathrm{sign}(a) + \mathrm{sign}(b)]\min(|a|,|b|)}{2}. \tag{50}$$

4.3. Geodesic advection

For a moving curve represented by the level set function ϕ, the value of ϕ does not change along the curve. If we apply this to the curve moving on the parameterization plane, we get

$$0 = \frac{\mathrm{d}\phi}{\mathrm{d}t} = \frac{\partial\phi}{\partial t} + \frac{\partial\phi}{\partial u^1}\underbrace{\frac{\mathrm{d}u^1}{\mathrm{d}t}}_{v_{u^1}} + \frac{\partial\phi}{\partial u^2}\underbrace{\frac{\mathrm{d}u^2}{\mathrm{d}t}}_{v_{u^2}} \tag{51}$$

with v_{u^i} being the speed of the curve in the direction of the parameter u^i. Comparing Eq. (51) with Eq. (45) yields

$$v_{u^1} = v_1 g^{11} + v_2 g^{12} \tag{52}$$

and

$$v_{u^2} = v_2 g^{22} + v_1 g^{12}. \tag{53}$$

An appropriate upwind numerical scheme for the component in the u^i direction is

$$v_{u^i}\phi_{u^i} \approx \max(v_{u^i}, 0)D_{u^i}^-\phi + \min(v_{u^i}, 0)D_{u^i}^+\phi. \tag{54}$$

5. Testing the numerical schemes

A curve evolution by geodesic curvature flow was implemented on a Klein bottle, see Fig. 3. This manifold has high curvature and is self-intersecting. In this case, the Klein bottle was parameterized according to Denise L. Chen's example shown in the Matlab software, where the two parts of the manifold (bulb and tube) use a separate parameterization. Therefore, this is a parametric manifold and not a non-orientable Klein bottle. The high order numerical scheme, combined with the regularizing process, yields a geodesic curvature flow without topological changes of the curve. See [28] for an analysis of such flows.

Geodesic constant flow is demonstrated in Fig. 4 for a section of a sphere and in Fig. 5 on the manifold $z = 0.5\sin(4\pi x)\sin(4\pi y)$. It is evident from the figures that the numerical scheme maintains its stability also at shocks.

Geodesic advection is demonstrated in Fig. 6 for a Klein bottle and in Fig. 7 for a section of a sphere.

6. Applications in image processing and computer vision

Geometric flows of curves on parametric manifolds have many applications. In this section we demonstrate their use in the areas of image processing and analysis. The first application consists of using the geodesic curvature flow to create a geometric scale space for images painted on manifolds. This has been previously done for manifolds that are function graphs [17]. The second application is the extension of the geodesic active contour model [12] to images painted on manifolds. This enables to use the manifold's geometry in order to improve the segmentation of the image painted on it.

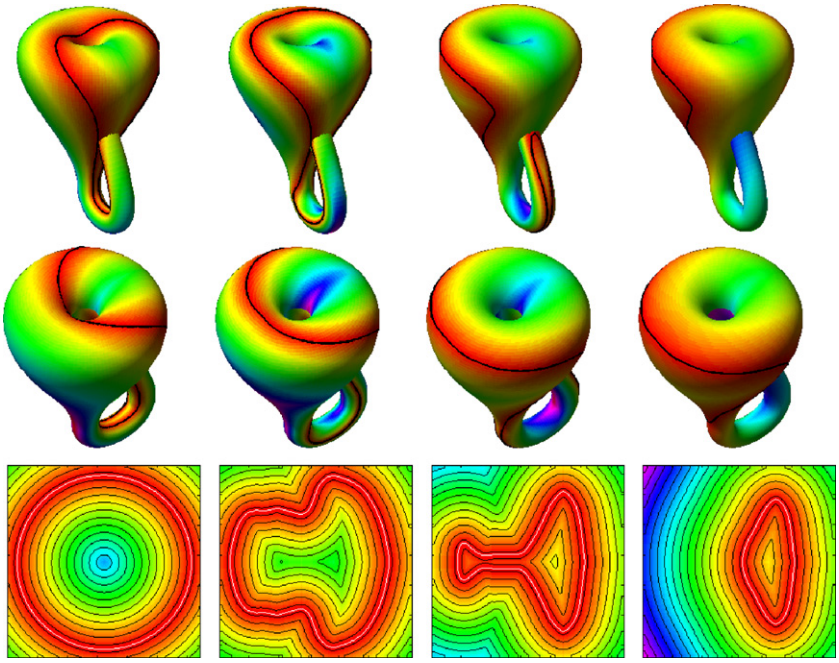

Fig. 3. Geodesic curvature flow on a Klein bottle. The two upper rows show the flow on the Klein bottle from two different viewing angles. The bottom row shows the flow on the parameterization plane. The colors (except for the white or black color of the curve) depict the values of the level set function. The black curves in the bottom row show the level curves of the level set function. (For interpretation of the references to colour in this figure legend, the reader is referred to the web version of this article.)

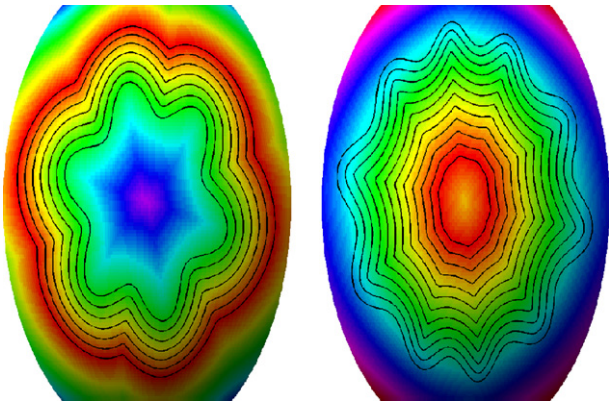

Fig. 4. Geodesic constant flow on a section of a sphere. On the left the curve is evolving outward and on the right inward. The black curves depict the location of the curve at various time steps. The other colors demonstrate the values of the level set function at the last iteration. (For interpretation of the references to colour in this figure legend, the reader is referred to the web version of this article.)

6.1. A geometric scale space for images painted on manifolds

The geodesic curvature flow can be applied to images painted on manifolds too. This creates an intrinsic scale space for the images on the manifolds [17]. Here we applied it to the image of the face of a mannequin painted on the mannequin's face manifold, see Fig. 8. The face manifold was originally a triangulated

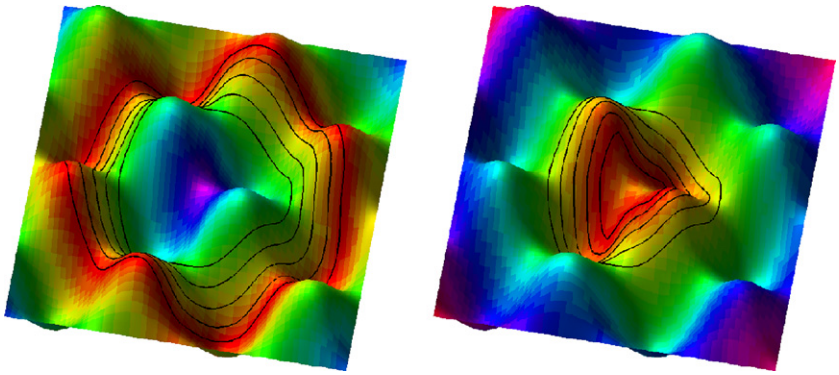

Fig. 5. Geodesic constant flow on the manifold $z = 0.5\sin(4\pi x)\sin(4\pi y)$. On the left the curve is evolving outward and on the right inward. The black curves depict the location of the curve at various time steps. The other colors demonstrate the values of the level set function at the last iteration. (For interpretation of the references to colour in this figure legend, the reader is referred to the web version of this article.)

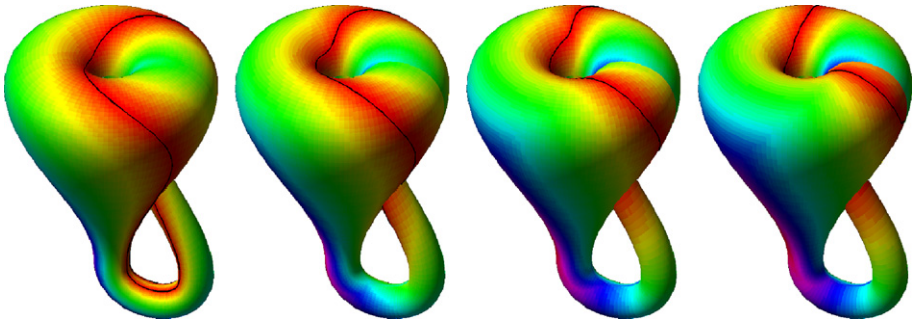

Fig. 6. Geodesic advection on a Klein bottle. The order of the images is from left to right. The colors (except for the black color of the curve) depict the values of the level set function. (For interpretation of the references to colour in this figure legend, the reader is referred to the web version of this article.)

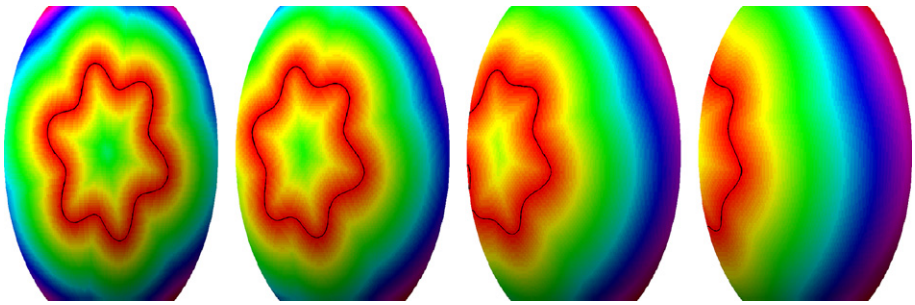

Fig. 7. Geodesic advection on a section of a sphere. The order of the images is from left to right. The colors (except for the black color of the curve) depict the values of the level set function. (For interpretation of the references to colour in this figure legend, the reader is referred to the web version of this article.)

manifold, generated by a 'home made' laser scanner [29]. In order to transform the manifold into a parametric manifold, the metric tensor has been approximated from the triangulated manifold. The approximation consisted of matching a second order polynomial patch at every grid point. The matching was done using singular value decomposition (SVD).

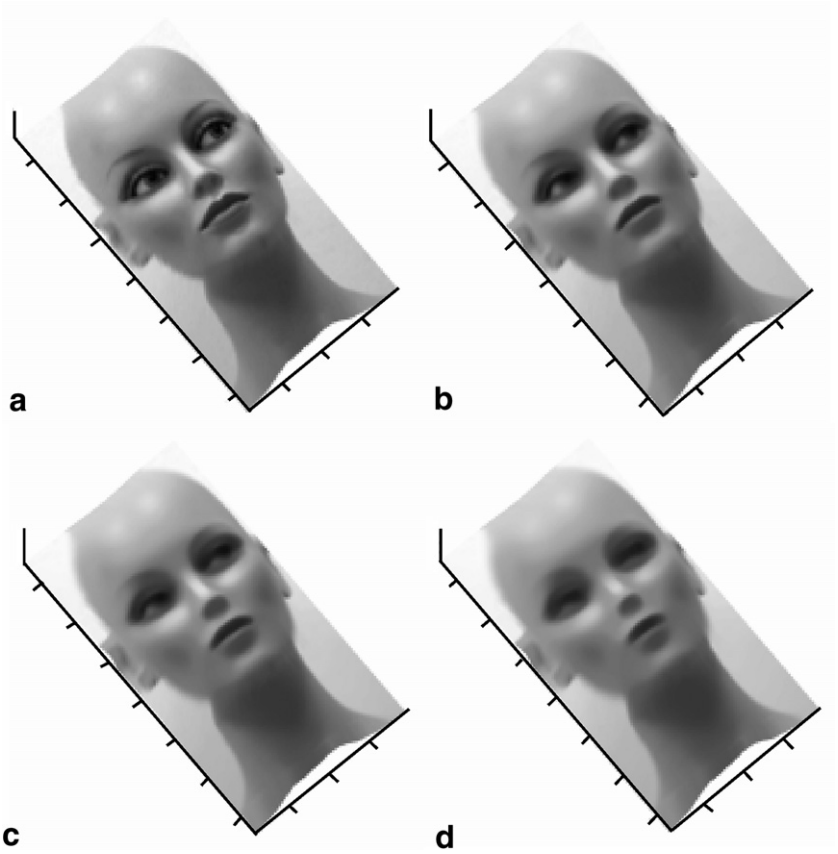

Fig. 8. Geodesic curvature flow of the face image on the face manifold.

6.2. Geodesic active contours on parametric manifolds

Active contours are a widely spread tool for the important task of image segmentation. An active contour evolves in time on an image, till it stops along the boundaries of the objects in it. The forces governing this evolution consist of internal geometric forces and external forces originating from the image data.

We present the use of active contours for the segmentation of a more general type of images, i.e. images painted on parametric manifolds. Good representatives of this kind of images are face images, where the face manifold is a two-dimensional manifold embedded in a Euclidean three-dimensional space. Adding the manifold data can be most beneficial in various tasks including face recognition where it enables a better segmentation of face features such as the eyes.

We show that taking into account the geometry of the manifold boosts the performance of active contours. The inclusion of the manifold's geometry is done by evolving the contour on the manifold, instead of on a flat planar image. In order to keep the contour on the manifold the geodesic components of the driving forces are used.

The active contours for image segmentation ('snakes') were introduced by Kass et al. [9]. Geometric active contours formulated and implemented based on the level set method [13] were presented by Caselless et al. [10] and Malladi et al. [11]. The first incorporation of a geometric (re-parameterization invariant) functional minimization was done in the geodesic active contour model of Caselless et al. [12] where the functional

$$\int_0^L f(C(s))\,\mathrm{d}s \tag{55}$$

using the edge sensitive weighting

$$f(|\nabla I|) = \frac{1}{1+\frac{|\nabla I|^2}{\lambda^2}} \tag{56}$$

of the image I is minimized by the Euler–Lagrange equations

$$C_t = (\kappa f - \langle \nabla f, N \rangle) N \tag{57}$$

with κ the curvature of the contour C, s its arc length, L its length and N its normal. The first term on the right-hand side of Eq. (57) is directly related to the geodesic curvature flow. The second term is geodesic advection. The level set representation [13] of the equation is

$$\phi_t = f \cdot \operatorname{div}\left(\frac{\nabla \phi}{|\nabla \phi|}\right)|\nabla \phi| + \langle \nabla f, \nabla \phi \rangle. \tag{58}$$

Additional developments followed, including [30–35].

The geodesic extension of Eq. (57) is

$$C_t = (\kappa_g f - \langle \nabla f, \widehat{N} \rangle)\widehat{N} \tag{59}$$

with $\widehat{N}$ the projection of the normal to the contour on the tangent plane to manifold M. The weighting function f stays as in Eq. (56). Replacing κ with κ_g in Eq. (57) and using $\widehat{N}$ instead of N are necessary in order to keep the active contour on the manifold.

The geodesic curvature flow, which is the first term on the right-hand side of Eq. (59), is a curve shortening flow. Its role is to contract the curve. The weighting function f that multiplies it stops the contraction at the image edges. The geodesic advection, which is the second term on the right-hand side of Eq. (59), is not active where the amplitude of the image edge ($|\nabla I|$) is constant since there $\nabla f = 0$. It comes into action in the vicinity of the edge and pulls the active contour to the maximum change of the intensity.

This flow is implemented numerically by performing the calculations on the parameterization plane. For the second term on the right-hand side of Eq. (59) we can identify V from Eq. (27) to be

$$V = \nabla f, \tag{60}$$

yielding

$$v_i \triangleq \langle V, X_i \rangle = \left\langle \left\{ \frac{\partial f}{\partial x^1}, \ldots, \frac{\partial f}{\partial x^N} \right\}, \left\{ \frac{\partial x^1}{\partial u^i}, \ldots, \frac{\partial x^N}{\partial u^i} \right\} \right\rangle = \frac{\partial f}{\partial u^i} \triangleq f_i. \tag{61}$$

Combining this with Eqs. (52) and (53) gives

$$v_{u^1} = g^{11} f_1 + g^{12} f_2 \tag{62}$$

and

$$v_{u^2} = g^{22} f_2 + g^{12} f_1. \tag{63}$$

Plugging this into Eq. (45) and using Eq. (37) for the first term on the right-hand side of Eq. (59) gives the following level set equation on the parameterization plane:

$$\phi_t = f\left[\frac{(-1)^{(i-j)}\phi_i \phi_j \phi_{(3-i)(3-j)}}{g|\nabla_M \phi|^2} + \frac{(-1)^{(i-j)} \Gamma_{ij}^k \phi_{(3-i)} \phi_{(3-j)} \phi_k}{g|\nabla_M \phi|^2}\right] + (f_m g^{mm} + f_{(3-m)} g^{12})\phi_m. \tag{64}$$

This equation is solved using the numerical schemes described in the previous section.

Fig. 9 shows the performance of the geodesic active contour model for an image painted on a Klein bottle. The image of a blurred square is painted on the parameterization plane and projected to the manifold to create the image appearing on the Klein bottle in the figure. The original contour is a concentric circle on the parameterization plane. It contracts till it stops on the edges of the square, thus segmenting it from the image's background.

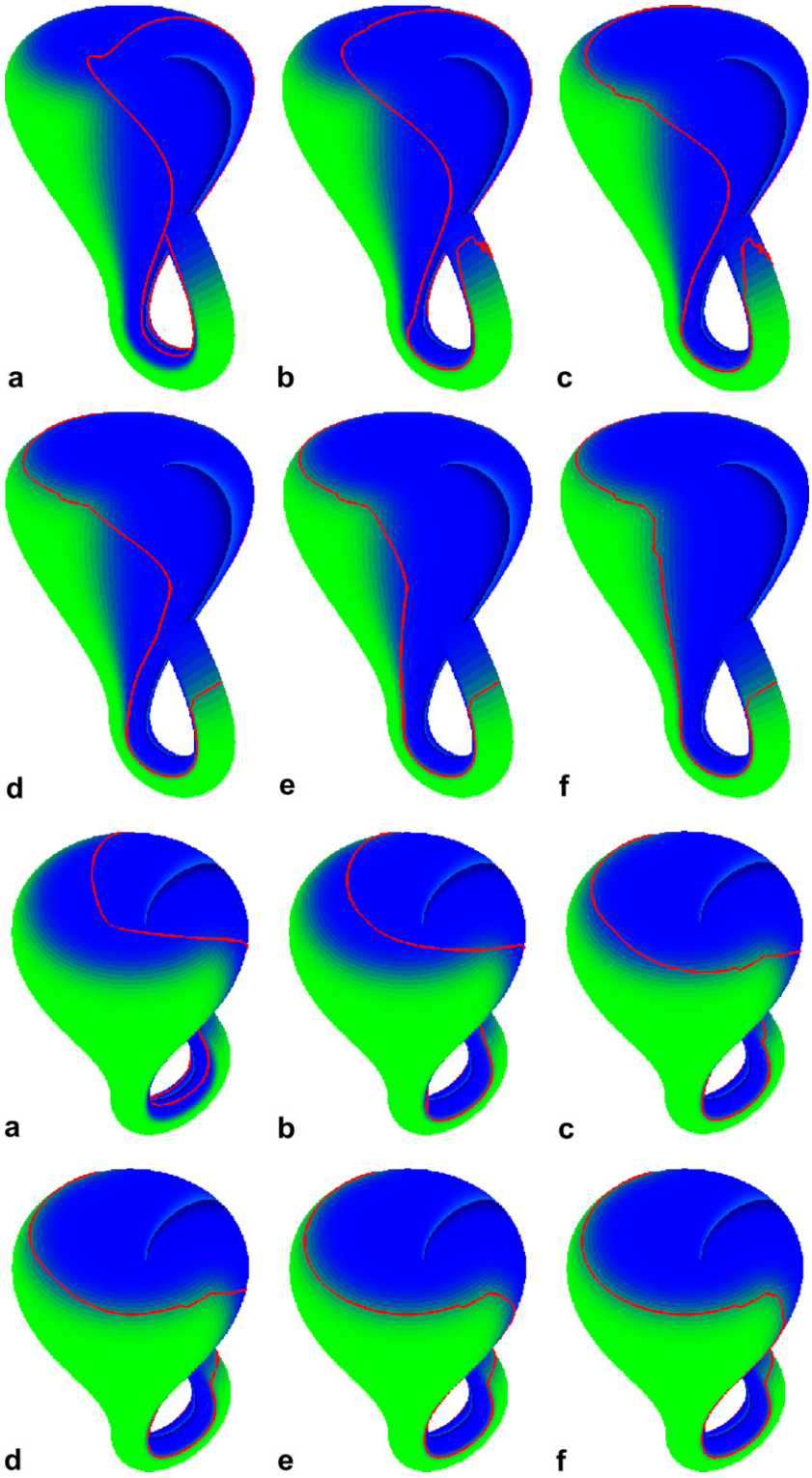

Fig. 9. The performance of the geodesic active contour model for an image painted on a Klein bottle. The segmented object is painted green on a blue background and the contour is red. The Klein bottle is shown from two viewing directions. (For interpretation of the references to colour in this figure legend, the reader is referred to the web version of this article.)

7. Conclusions

We introduced level set formulations and their corresponding numerical schemes for the implementation of various geometric flows of curves on parametric manifolds. The implementation of the schemes on the parameterization plane of the manifold is the source of their efficiency and robustness.

The flows were then used for creating a scale space for images painted on manifolds and for implementing the geodesic active contour model for the segmentation of this kind of images.

References

[1] B. ter Haar Romeny, Geometry-Driven Diffusion in Computer Vision, Kluwer Academic Publishers, Dordrecht, Netherlands, 1994.
[2] L. Alvarez, F. Guichard, P. Lions, J. Morel, Axioms and fundamental equations of image processing, Arch. Rat. Mech. Anal. 16 (9) (1993) 200–257.
[3] P. Perona, J. Malik, Scale-space and edge detection using anisotropic diffusion, IEEE Trans. Pattern Anal. Mach. Intell. 12 (1990) 629–639.
[4] G. Sapiro, A. Tannenbaum, Affine invariant scale-space, Int. J. Comput. Vis. 11 (1) (1993) 25–44.
[5] L. Alvarez, P. Lions, J. Morel, Image selective smoothing and edge detection by nonlinear diffusion, SIAM J. Numer. Anal. 29 (1992) 845–866.
[6] L. Rudin, S. Osher, E. Fatemi, Nonlinear total variation based noise removal algorithms, Physica D 60 (1992) 259–268.
[7] N. Sochen, R. Kimmel, R. Malladi, A general framework for low level vision, IEEE Trans. Image Process. 7 (3) (1998) 310–318.
[8] J. Weickert, Anisotropic Diffusion in Image Processing, Teubner-Verlag, Stuttgart, Germany, 1998.
[9] M. Kass, A. Witkin, D. Terzopoulos, Snakes: active contour models, Int. J. Comput. Vis. 1 (1988) 321–331.
[10] V. Caselles, F. Catte, T. Coll, F. Dibos, A geometric model for active contours, Numer. Math. 66 (1993) 1–31.
[11] R. Malladi, J. Sethian, B. Vemuri, Shape modeling with front propagation: a level set approach, IEEE Trans. Pattern Anal. Mach. Intell. 17 (2) (1995) 158–175.
[12] V. Caselles, R. Kimmel, G. Sapiro, Geodesic active contours, Int. J. Comput Vis. 22 (1) (1997) 61–79.
[13] S. Osher, J. Sethian, Fronts propagation with curvature dependent speed: algorithms based on Hamilton–Jacobi formulations, J. Comput. Phys. 79 (1988) 12–49.
[14] D. Chopp, J. Sethian, Flow under curvature: singularity formation, minimal surfaces, and geodesies, J. Exper. Math. 2 (4) (1993) 235–255.
[15] R. Kimmel, A. Amir, A. Bruckstein, Finding shortest paths on surfaces using level sets propagation, IEEE Trans. PAMI 17 (1) (1995) 635–640.
[16] R. Kimmel, N. Kiryati, Finding shortest paths on surfaces by fast global approximation and precise local refinement, Int. J. Pattern Recognit. Arti. Intell. 10 (6) (1996) 643–656.
[17] R. Kimmel, Intrinsic scale space for images on surfaces: the geodesic curvature flow, Graph. Models Image Process. 59 (5) (1997) 365–372.
[18] T. Barth, J.A. Sethian, Numerical schemes for the Hamilton–Jacobi and level set equations on triangulated domains, J. Comput. Phys. 145 (1) (1998) 1–40.
[19] L. Cheng, P. Burchard, B. Merriman, S. Osher, Motion of curves constrained on surfaces using a level set approach, J. Comput. Phys. 175 (2) (2002) 604–644.
[20] M. Bertalmio, L. Cheng, S. Osher, G. Sapiro, Variational problems and partial differential equations on implicit surfaces, J. Comput. Phys. 174 (2001) 759–780.
[21] A. Spira, R. Kimmel, Geodesic curvature flow on parametric surfaces, in: Curve and Surface Design: Saint-Malo 2002, Saint-Malo, France, 2002, pp. 365–373.
[22] A. Spira, R. Kimmel, Segmentation of images painted on parametric manifolds, in: Eusipco 2005, Antalya, Turkey, 2005.
[23] M.D. Carmo, Differential Geometry of Curves and Surfaces, Prentice-Hall, New Jersy, USA, 1976.
[24] G. Jiang, D. Peng, Weighted ENO schemes for Hamilton–Jacobi equations, SIAM J. Sci. Comput. 21 (6) (2000) 2126–2143.
[25] C. Shu, Total-variation-diminishing time discretizations, SIAM J. Sci. Stat. Comput. 9 (6) (1988) 1073–1084.
[26] M. Sussman, E. Fatemi, An efficient interface preserving level set re-distancing algorithm and its application to interfacial incompressible fluid flow, SIAM J. Sci. Comput. 20 (4) (1999) 1165–1191.
[27] E. Rouy, A. Tourin, A viscosity solutions approach to shape-from-shading, SIAM J. Numer. Anal. 29 (3) (1992) 867–884.
[28] M. Grayson, Shortening embedded curves, Ann. Math. 129 (1989) 71–111.
[29] G. Zigelman, R. Kimmel, N. Kiryati, Texture mapping using surface flattening via multi-dimensional scaling, IEEE Trans. Visual. Comput. Graphics 8 (2) (2002) 198–207.
[30] R. Malladi, J. Sethian, An $O(N\log(N))$ algorithm for shape modeling, Proc. Natl. Acad. Sci. 93 (1996) 9389–9392.
[31] V. Caselles, R. Kimmel, G. Sapiro, C. Sbert, Minimal surfaces based object segmentation, IEEE Trans. Pattern Anal. Mach. Intell. 19 (4) (1997) 394.
[32] T. Chan, L. Vese, Active contours without edges, IEEE Trans. Image Process. 10 (2) (2001) 266–277.

[33] R. Goldenberg, R. Kimmel, E. Rivlin, M. Rudsky, Fast geodesic active contours, IEEE Trans. Image Process. 10 (10) (2001) 1467–1475.
[34] R. Kimmel, A. Bruckstein, On regularized Laplacian zero crossings and other optimal edge integrators, Int. J. Comput. Vis. 53 (3) (2003) 225–243.
[35] B. Gilburd, M. Holtzman-Gazit, A. Spira, D. Goldsher, R. Kimmel, Volumetric medical imaging environment, in: Proceedings of Dicta 2003, Sydney, Australia, 2003.